

## Investigation of contact electrification based broadband energy harvesting mechanism using elastic PDMS microstructures

This content has been downloaded from IOPscience. Please scroll down to see the full text.

2014 J. Micromech. Microeng. 24 104002

(<http://iopscience.iop.org/0960-1317/24/10/104002>)

View [the table of contents for this issue](#), or go to the [journal homepage](#) for more

Download details:

IP Address: 137.132.123.69

This content was downloaded on 23/09/2014 at 15:15

Please note that [terms and conditions apply](#).

# Investigation of contact electrification based broadband energy harvesting mechanism using elastic PDMS microstructures

Lokesh Dhakar<sup>1, 2</sup>, F E H Tay<sup>2, 3</sup> and Chengkuo Lee<sup>1</sup>

<sup>1</sup> Department of Electrical and Computer Engineering, National University of Singapore, 4 Engineering Drive 3, Singapore 117576, Singapore

<sup>2</sup> NUS Graduate School for Integrative Sciences and Engineering

<sup>3</sup> Department of Mechanical Engineering, National University of Singapore, 9 Engineering Drive 1, Singapore 117576, Singapore

E-mail: [elelc@nus.edu.sg](mailto:elelc@nus.edu.sg)

Received 4 April 2014, revised 30 May 2014

Accepted for publication 3 June 2014

Published 22 September 2014

## Abstract

Triboelectric energy harvesting has recently garnered a lot of interest because of its easy fabrication and high power output. Contact electrification depends on the chemical properties of contacting materials. Another important factor in contact electrification mechanism is surfaces' elastic and topographical characteristics. One of the biggest limitations of resonant mechanism based devices is their narrow operating bandwidth. This paper presents a broadband mechanism which utilizes stiffness induced in the cantilever motion due to contact between two triboelectric surfaces. We have conducted experiments using polydimethylsiloxane (PDMS) micropad patterns to study the effect of micropad array configuration on the performance of triboelectric energy harvesting devices. The maximum power output measured from the device was observed to be  $0.69 \mu\text{W}$  at an acceleration of 1 g. Due to the non-linearity introduced by contact separation mechanism, the bandwidth of the triboelectric energy harvester was observed to be increased by 63% at an acceleration level of 1 g. A hybrid energy harvesting mechanism has also been demonstrated by compounding the triboelectric energy harvester with a piezoelectric bimorph.

Keywords: broadband, contact electrification, triboelectric energy harvester, micropatterns

(Some figures may appear in colour only in the online journal)

## 1. Introduction

In recent years, energy harvesting has emerged as a practicable solution for powering low power electronic devices [1, 2] and various kind of wireless sensors [2–4]. As the power output of the energy harvesting solution increases, they could potentially replace batteries in some of the applications in sensors and electronic devices. Traditionally, researchers have most commonly used piezoelectric [5–10], electromagnetic [11–15] and electrostatic [16, 17] mechanisms to harvest mechanical energy from vibrations and pressure available in

the environment. In the past few years, contact electrification or triboelectric mechanism has also gained interest as a mechanism for harvesting mechanical energy [18–26]. The word triboelectricity comes from two words *tribein* which means to rub in Greek and *electricity*. Therefore triboelectricity means electricity generated by rubbing or in other words generating electricity using friction. As per the triboelectric effect, two materials become charged as they come in contact and separate with each other. There have been many studies conducted to study the triboelectric effect between various combination of materials. The tendency of two dissimilar materials to get

charged when they are put in contact with each other can be explained by the difference in the electronegativity of the two materials. Materials can be arranged in an order or series according to their tendency to donate and attract electrons. This series is known as triboelectric series [27, 28] and comprises of materials with higher tendency to donate electrons up in the series while the materials with higher tendency to accept electrons are placed down in the series.

For resonant behavior based energy harvesting devices, one of the biggest limitations has been a narrow operating bandwidth within which the devices can generate significant power. As soon as the device is excited with frequency outside the operating bandwidth, the power output drops drastically and the energy harvesting device is virtually rendered useless. In energy harvesting devices based on piezoelectric, electromagnetic and electrostatic mechanisms, various strategies have been used to broaden the operating bandwidth of resonant behavior based devices. Sebald *et al* [29] used magnetic interactions to induce nonlinearities which resulted in broadband behavior. Stanton *et al* [30] used bistable mechanism in piezoelectric energy harvester resulting in increased capability of device to respond to broad frequency range. Huan *et al* [31] used an array of bimorphs with different operating frequencies leading to overall broad operating frequency range. Nguyen *et al* [32] used softening springs in MEMS based electrostatic energy harvester to induce broadband behavior. Soliman *et al* [33] used piecewise linear oscillator which resulted into observation of broadband behavior in energy harvesting device. All these strategies and designs have been aimed towards solving one of important problems in resonant mechanism based energy harvesters, i.e. narrow operating bandwidth which hugely restricts the devices operability.

The current design uses contact separation mechanism of triboelectric layers to induce stiffening in the mechanical motion of the cantilever. This stiffening of the cantilever has been demonstrated to broaden the operating bandwidth of a triboelectric energy harvester (TEH). We discuss the fabrication of triboelectric mechanism energy harvesting devices. We also study the effect of array configuration of micropad patterns in the triboelectric layer on the performance of triboelectric energy harvesting mechanism. A hybrid energy harvester concept has also been demonstrated which uses a piezoelectric bimorph to mount one of the triboelectric layers. The hybrid concept used both piezoelectric mechanism and triboelectric mechanism in conjunction. Several hybrid mechanisms have been demonstrated before which use two different mechanisms in order to improve the efficiency of overall energy harvesting mechanism [34].

## 2. Device design

### 2.1. Fabrication of the triboelectric layers

The TEH comprises of two triboelectric layers (figure 1) made of different materials which generate charges using contact electrification mechanism. The first triboelectric layer

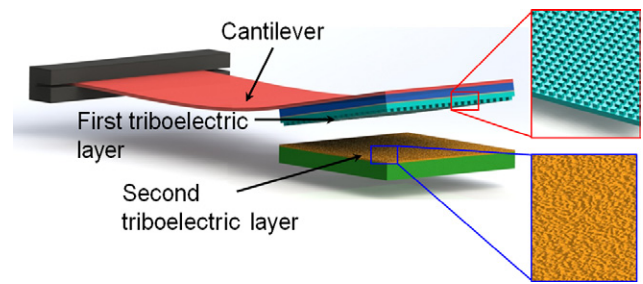


**Figure 1.** Schematic illustration of the broadband triboelectric energy harvester.

is made of PDMS micropad structures. The process flow for fabrication of PDMS micropad structures is shown in detail in figure 2(a). To prepare the first triboelectric layer, silicon wafer with oxide layer is cleaned using acetone and IPA followed by oxygen plasma. After cleaning, the samples are spin coated with hexamethyldisilazane (HMDS) followed by spin coating of AZ9260. Then the sample is baked at a temperature of 110 °C for 30 min. Thereafter, the photoresist is exposed using mask to perform the photolithography. The samples are then again baked at a temperature of 120 °C for 30 min. The samples are then developed in AZ developer for 12 min. After patterning the AZ9260 photoresist, the photoresist patterns are used as mold to fabricate PDMS micropad structures. To transfer the micropad patterns on the PDMS, SYLGARD® 184 silicone elastomer kit is used. The base and the curing agent are mixed in a 10:1 ratio and the mixture is degassed in a vacuum chamber for 2 h to remove the air bubbles introduced during the mixing. After degassing, the PDMS mixture is spin coated on the silicon mold and then cured at 85 °C for 1 h. After curing the PDMS mixture, the PDMS layer can be peeled off and micropad structures can be seen on the PDMS layer. This patterned PDMS layer is then attached to a glass slide coated with 100 nm thick layer of Cu as shown in steps in figure 2(a) (ii). For attaching, an uncured layer of PDMS is spin coated on the glass slide and again cured together after laying the patterned PDMS layer on it. The copper thin film on the glass slide acts as the first electrode for the TEH. Figure 2(b) shows the optical image of the patterned PDMS layer on top of the copper thin film.

For the second triboelectric layer of TEH, a glass substrate is laid with a 40 μm thick laminated copper layer. The copper surface is treated with Ar/O<sub>2</sub> plasma at 70 W for 1 h to create nano-roughness as shown in the AFM image in figure 2(c). The roughness created by plasma treatment is used to improve the triboelectric properties of the second triboelectric layer.

### 2.2. Assembling the TEH

After fabrication of both parts, the first part with the micropad patterned PDMS triboelectric layer is attached to an aluminum metal cantilever using epoxy adhesive (figure 1). An aluminum cantilever is used as it suitably provides stable mechanical vibrations necessary for contact-separation mechanism of the two triboelectric layers. The metal cantilever is excited using external mechanical vibrations due to which first triboelectric,

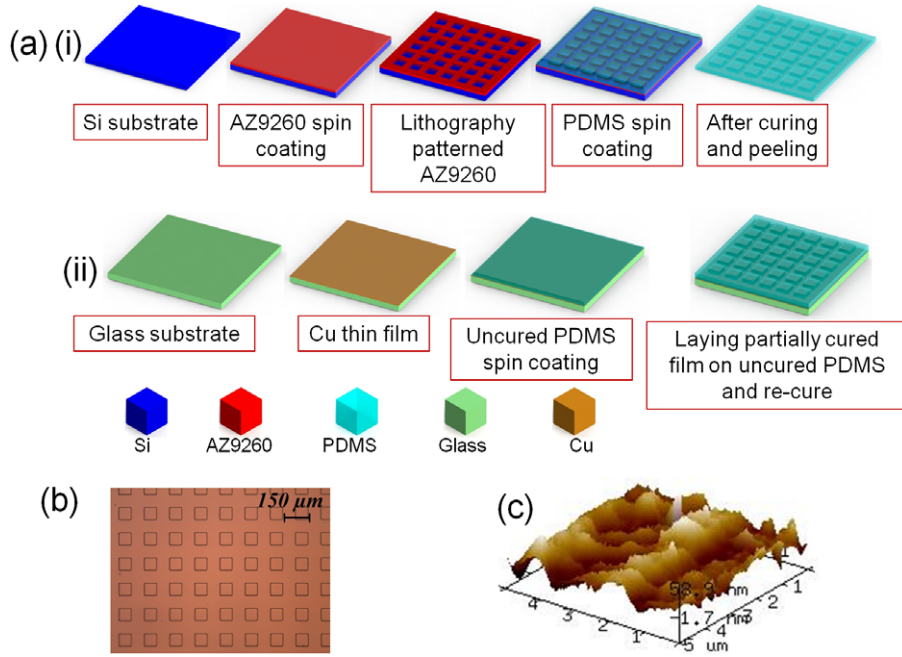


**Figure 2.** (a) Fabrication of top triboelectric layer in the triboelectric energy harvesting device. (b) Optical image of the first triboelectric layer with patterned elastic PDMS micropads on top of copper thin film. (c) AFM image of the second triboelectric layer with Ar/O<sub>2</sub> plasma treated copper layer to create nano-roughness.

i.e. patterned PDMS layer undergoes regular contact-separation motion with the second triboelectric layer.

### 3. Theory and modeling

#### 3.1. Mechanical modeling of microstructures

When the two triboelectric layers come in contact with each other, the surface charge generated depends on two factors: (i) chemical properties of materials and (ii) surface topography of triboelectric layers. To enhance the triboelectric effect using the surface topography, cuboidal shaped PDMS micropad patterns structures were fabricated (figure 2(b)). Micropad structures were chosen over high aspect ratio PDMS pillars because during the contact-separation mechanism required for contact electrification process, high aspect ratio PDMS pillars tend to collapse [35], which may lead to deterioration of performance of the TEH after a certain number of operating cycles.

The micropad structures can be modeled using the generalized Hooke law in three dimensions as expressed in equation (1). It is assumed that PDMS is a homogenous material, which means the mechanical properties of PDMS are not direction dependent.

$$\begin{bmatrix} \epsilon_{xx} \\ \epsilon_{yy} \\ \epsilon_{zz} \end{bmatrix} = \begin{bmatrix} \frac{1}{E} & -\frac{\nu}{E} & -\frac{\nu}{E} \\ -\frac{\nu}{E} & \frac{1}{E} & -\frac{\nu}{E} \\ -\frac{\nu}{E} & -\frac{\nu}{E} & \frac{1}{E} \end{bmatrix} \begin{bmatrix} \sigma_{xx} \\ \sigma_{yy} \\ \sigma_{zz} \end{bmatrix} \quad (1)$$

where  $\epsilon_{ii}$  is the strain in direction  $i = x, y, z$ ,  $\sigma_{ii}$  is the normal stress in direction  $i = x, y, z$ ,  $E$  is the Young's modulus

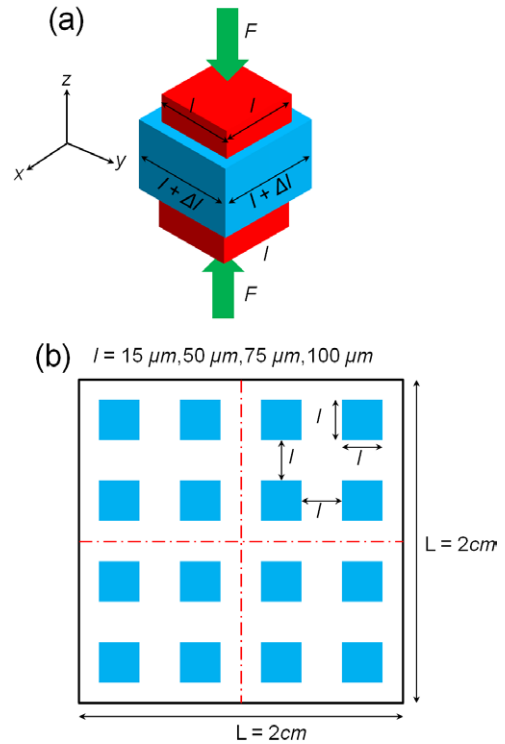


**Figure 3.** (a) Deformation in PDMS pad type structures when mechanical force is applied. (b) Schematic of PDMS micropad array in a square lattice.

and  $\nu$  is Poisson's ratio. If we assume that in the contact separation mechanism normal stress is applied in only normal  $z$ -direction on the PDMS micropad structures as shown in figure 3(a), the other two normal stress terms in equation (1), i.e.  $\sigma_{xx}$  and  $\sigma_{yy}$  disappear from equation (1).

Therefore, from equation (1) following set of equations can be derived:

$$\epsilon_{xx} = -\frac{\nu}{E}\sigma_{zz}, \quad \epsilon_{yy} = -\frac{\nu}{E}\sigma_{zz}, \quad \epsilon_{zz} = \frac{1}{E}\sigma_{zz} \quad (2)$$

Figure 3(b) illustrates a schematic diagram of micropad array pattern in a square lattice. The total square sample size, i.e. micropad array size has a side length of  $L$ . Each individual micropad has a square cross-section of side length  $l$ . The gap between two micropads along both  $x$ -axis and  $y$ -axis is also equal to  $l$ . The elastic deformation in the PDMS micropad structures along  $x$ -axis and  $y$ -axis can be calculated as:

$$\Delta x = l\epsilon_{xx} = -\frac{l}{E}\nu\sigma_{zz}$$

$$\Delta y = l\epsilon_{yy} = -\frac{l}{E}\nu\sigma_{zz} \quad (3)$$

The change in total contact area between two triboelectric layers due to the elastic deformation in the PDMS micropad structure can be calculated as in equation (4).

$$\Delta A = \Delta x \times \Delta y = \frac{l^2}{E^2}\nu^2\sigma^2 \quad (4)$$

The change in the total effective contact area after elastic deformation is hence given by:

$$n \times \Delta A = \left(\frac{L}{2l}\right)^2 \times \frac{l^2}{E^2}\nu^2\sigma^2 = \frac{L^2\nu^2\sigma^2}{4E^2} \quad (5)$$

where  $n$  is the total number of pillar on the PDMS triboelectric layer and is equal to  $\left(\frac{L}{2l}\right)^2$ . It is clear from equation (5) that theoretically the effective change in the contact area after the elastic deformation is independent of the dimension  $l$  in micropad arrays (figure 3(b)).

### 3.2. Contact analysis of two triboelectric layers

The average impact force between the two triboelectric layers depends on the momentum change of the piezoelectric bimorph and the duration of impact between two triboelectric layers. The equation for impact force can be written as:

$$F_{\text{impact}} = \frac{\Delta P}{\Delta T} \quad (6)$$

where  $\Delta P$  is the change in momentum of the cantilever and  $\Delta T$  is the time duration of impact between the two triboelectric layers. From the Hertz theory of contact mechanics, it is predicted that the duration of impact  $\Delta T$  increases as the overall elasticity of triboelectric layer increases or the stiffness decreases [36, 37]. The equivalent stiffness of the PDMS triboelectric layer with micropad patterns can be calculated using springs acting in parallel relation:

$$k_{\text{eff}} = \sum_{i=1}^n k_i \quad (7)$$

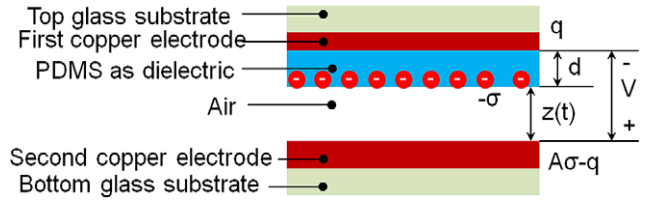


Figure 4. Modeling of the TEH as a parallel plate capacitor system with varying gap.

where  $k_{\text{eff}}$  is the effective spring constant of the triboelectric layer with PDMS pad patterns and  $k_i$  is the spring constant of an individual PDMS micropad.

The spring constant for an individual micropad can be obtained by using Hooke's law as below:

$$k_i = \frac{El^2}{h} \quad (8)$$

where  $l$  is the side length of cross section of the square micropad structure and  $h$  is the height of the micropad structure. Now, the effective spring constant can be calculated from equation (7):

$$k_{\text{eff}} = n \times k_i = \left(\frac{L}{2l}\right)^2 \times \frac{El^2}{h} = \frac{EL^2}{4h} \quad (9)$$

In the experiments, we fabricated five sets of devices: one with plain/unpatterned and four others that used four different array configurations of micropad structures. Figure 3(b) illustrates a schematic diagram of the micropad pattern arrays fabricated. Equation (9) suggests that the effective stiffness of PDMS triboelectric layer is the same for all the array configurations as  $k_{\text{eff}}$  is independent of the dimensional parameter  $l$  is the side length of individual square micropad. This means that the duration of impact  $\Delta T$  should remain the same for all array configurations. Hence the impact force should also remain the same for a given value of momentum change, as given by equation (6).

### 3.3. Modeling of the TEH as a parallel plate capacitor system with varying gap

Behind the working of the TEH, there are two mechanisms involved, namely contact electrification or triboelectrification and electrostatic induction of charges. The mechanism involves charging of triboelectric layers with equal and opposite charge when they come in contact with each other due to vibration of the cantilever. The charges on the PDMS layer can be assumed to be uniformly distributed over the surface [38]. These triboelectric charges on the PDMS triboelectric layer result in electrostatically induced charges on the first copper electrode. The electrodes and triboelectric layer can be approximated by using a system of parallel plate capacitors as shown in figure 4. The potential difference between the first and second copper electrodes is given by equation (10).

$$V = -\frac{q}{A\epsilon_0} \left( \frac{d}{\epsilon_p} + z(t) \right) + \frac{\sigma z(t)}{\epsilon_0} \quad (10)$$

where  $V$  is the potential difference between the first and second copper electrode,  $A$  is the total area of the triboelectric layers,  $d$  is the thickness of PDMS dielectric layer,  $\epsilon_0$  is the

dielectric constant of air,  $\epsilon_p$  is the relative dielectric constant of PDMS,  $z(t)$  is the time varying distance between the PDMS layer and the second copper electrode,  $\sigma$  is the triboelectric charge density due to contact electrification mechanism and  $q$  is the charge transferred through the external circuit.

For the calculation of open circuit voltage, there should not be any charge transfer in the external circuit which gives the condition  $q = 0$  in equation (10). Therefore open circuit voltage is given by equation (11).

$$V_{OC} = \frac{\sigma z(t)}{\epsilon_0} \quad (11)$$

For the calculation of short circuit current, the potential difference between the first and second electrode should be zero, i.e.  $V = 0$  in equation (10). This gives the following equation:

$$q = \frac{A\sigma\epsilon_p z(t)}{d + \epsilon_p z(t)} \quad (12)$$

Therefore the short circuit current can be calculated as given by equation (13).

$$I_{SC} = \frac{dq}{dt} = \frac{A\sigma\epsilon_p d}{(d + \epsilon_p z(t))^2} v(t) \quad (13)$$

where  $v(t) = dz(t)/dt$  which means the velocity of the tip of vibrating cantilever.

### 3.4. Modeling of broadband behavior

The modeling of broadband behavior can be done using the piecewise linear oscillator model as shown below [39, 40]:

$$\ddot{x} + 2\zeta_0\dot{x} + x = r^2 \sin(r\tau) + f_1(x, \dot{x}) \quad (14)$$

The expression for  $f_1(x, \dot{x})$  is given by:

$$f_1(x, \dot{x}) = \begin{cases} -2r_1\zeta_1\dot{x} - r_1^2x + r_1^2\delta_1, & x \geq d_0 \\ 0, & x < d_0 \end{cases} \quad (15)$$

where  $r = \omega / \omega_0$ ,  $r_1 = \omega_1 / \omega_0$ ,  $u = z / Y$ ;  $\delta_1 = d / Y$ ;  $\omega_0$  and  $\omega_1$  are resonant frequency before and after the contact of two triboelectric layers;  $Y$  is the amplitude of sinusoidal excitation provided by shaker; and  $\zeta_0$  and  $\zeta_1$  are damping coefficients before and after the contact of two triboelectric layers. The equations were solved and simulated using MATLAB and the results are plotted in figure 5 for acceleration value of 1 g. Figure 5 explains the behavior of cantilever motion due to nonlinearity introduced in the cantilever vibration by contact-separation mechanism of the two triboelectric layers.

## 4. Experiments and discussion

### 4.1. Experimental setup

For testing the TEH characteristics, a test setup was assembled. The setup comprised of an electromagnetic shaker (B&K Vibration Exciter Type 4809) which simulated the vibrations at different acceleration levels. The shaker is driven by using a computer program which sends signal to a power amplifier (B&K Power Amplifier Type 2718). From the power

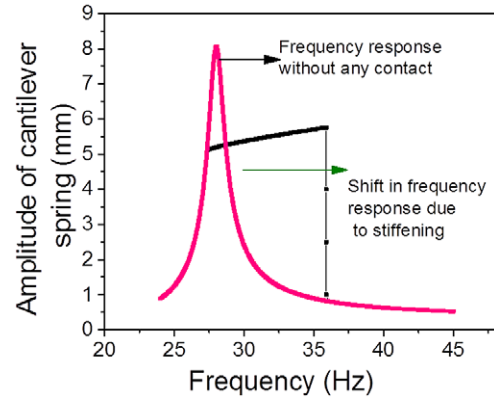


**Figure 5.** Simulation of broadband behavior due to contact-separation mechanism of triboelectric layers.

amplifier, signal is sent to electromagnetic shaker to simulate vibrations. The acceleration level provided by the shaker is measured using an accelerometer (DeltaTron® accelerometer Type 4519–003) which is again sent to a computer program via a vibration controller as a feedback loop to control the acceleration level of the shaker. A computer program is used to perform two operations: sweeping frequency and dwell at a constant frequency at various acceleration levels. The TEH is assembled on the shaker and the signal is acquired by a data acquisition system via a vibration control channel which is then transferred to the computer using an ethernet port. Figure 6 shows a schematic of the test setup.

### 4.2. Design of experiment

PDMS micropad pattern arrays were used to enhance the triboelectric effect between the two triboelectric layers. Five variations of TEH devices were prepared which included one with plain/unpatterned PDMS layer and four others with different array configuration as shown in figure 3(b). The array dimensions were carefully chosen such that the contact area due to the micropad top surface as a percentage of total sample size is equal for all the array patterns. This is illustrated by the following calculations:

$$\text{Total number of micropads} = \frac{L}{2l} \times \frac{L}{2l}$$

$$\text{Total micropad area} = \frac{L}{2l} \times \frac{L}{2l} \times l^2 = 0.25L^2$$

$$\text{Total micropad area as \% of sample size}$$

$$= \frac{0.25L^2}{L^2} \times 100\% = 25\% \quad (16)$$

From equation (16), it is clear that the total contact area due to micropad top surface before the elastic deformation in the micropad is same for all the array configurations, which is  $0.25L^2$ .

### 4.3. Broadband behavior of the TEH

Broadband behavior was observed in the TEH due to stiffening of the cantilever spring introduced by the fixed second

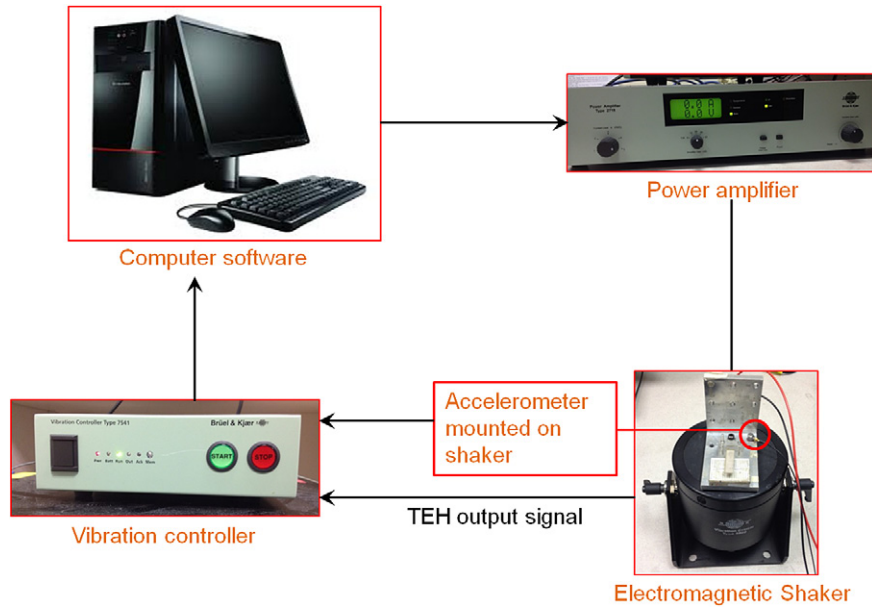


Figure 6. Flow chart for the experimental setup to test the TEH.

triboelectric layer as the first layer comes in contact. The broadband behavior can be studied by up-sweeping and down-sweeping of frequency, as shown in figure 7 which shows the results for the micropad array of the  $50\mu\text{m} \times 50\mu\text{m}$  sample. An additional mass of 2.36 gram was attached at the cantilever tip for all the experiments to increase the proof mass. When a down-sweep of the frequency is conducted, the resonant frequency of the device is observed to be  $\sim 31.5\text{Hz}$ . However, when the up-sweep of frequency is conducted, broadband characteristic of the TEH can be observed. During the up-sweeping, as the first triboelectric layer attached on cantilever spring comes in contact with the second triboelectric layer, the stiffening occurs in the cantilever spring and hence the effective spring constant increases. Due to increase in the effective spring constant the resonant frequency of the device increases which further shifts the resonant peak to the right of the original resonant peak. In figure 7, as the frequency increases from 31.5 Hz to 38.8 Hz, the effective stiffness increases and the TEH operating frequency range keeps broadening till point A, as shown in figure 7. Thereafter, the output voltage drops abruptly [33] and both the triboelectric layers lose contact with each other for further increase in operating frequency. The operating bandwidth for excitation acceleration of 1 g at a voltage level of 70 mV RMS output voltage increased from 7.3 Hz to 11.9 Hz which is an increment of 63% from the original operating bandwidth.

Furthermore, experiments were conducted to study the broadband behavior in the TEH with different PDMS micropad dimensions at different excitation acceleration levels. Figure 8 shows the results of RMS output voltage generated by five different TEH devices with an additional proof mass of 2.36 gram. For all the devices, the excitation acceleration level is increased from 0.6 g to 1.4 g in steps of 0.2 g. It can be observed that for all five samples that as the acceleration level is increased, the operating bandwidth also increases along with increased output level.

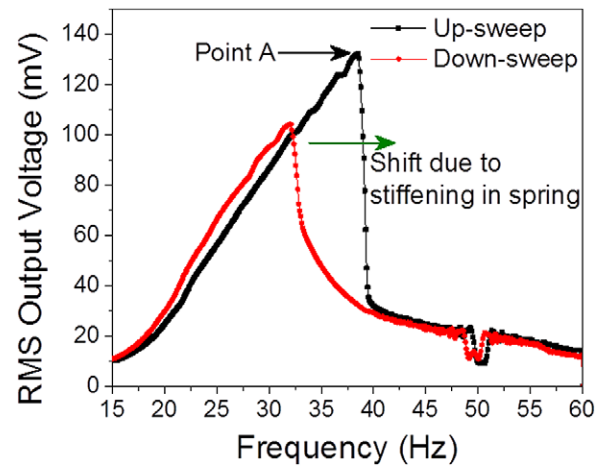
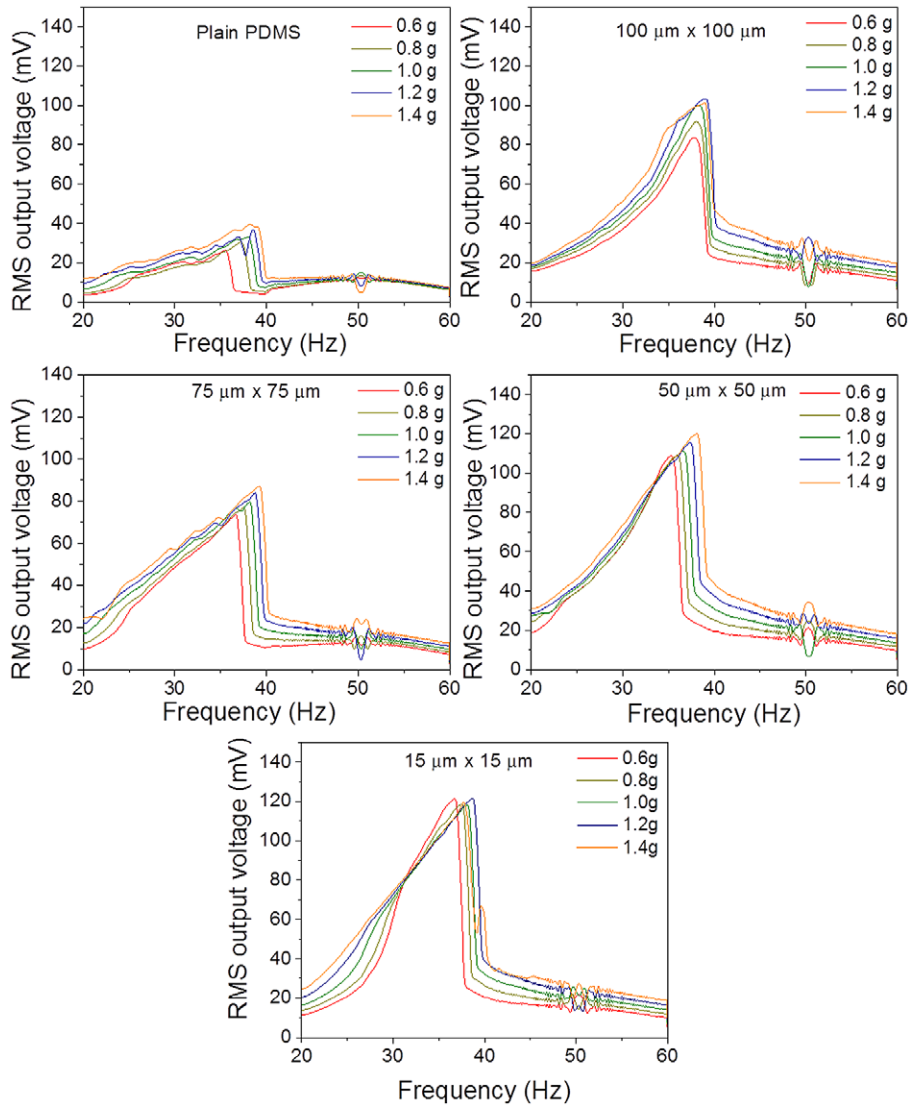


Figure 7. RMS output voltage for frequency up-sweep and down-sweep at an acceleration level of 1 g for  $50\mu\text{m} \times 50\mu\text{m}$  sample.

#### 4.4. TEH output characteristics

Output voltage and current were measured for the TEH with micropad dimension of  $50\mu\text{m} \times 50\mu\text{m}$  at various values of load resistances connected to the TEH. The voltage and current characteristics for  $50\mu\text{m} \times 50\mu\text{m}$  micropad dimensions at acceleration level of 1 g are summarized in figure 9. All the measurements were conducted with an additional proof mass of 2.36 gram. The results are presented for only one device sample as the characteristics for other devices would also follow the same qualitative pattern. The output voltage across the load resistance increases as the load resistance value is increased from  $50\text{k}\Omega$  to  $11\text{M}\Omega$ . The current flowing through the resistor follows a reverse trend as compared to the output voltage across the resistor. The current flowing through the load resistor decreases as the load resistance value is increased.

Figure 10(a) shows the power characteristics of the TEH device with micropad dimensions of  $50\mu\text{m} \times 50\mu\text{m}$  at an



**Figure 8.** Broadband characteristics of the TEH observed due to nonlinearity induced due to contact-separation mechanism between two triboelectric layers.

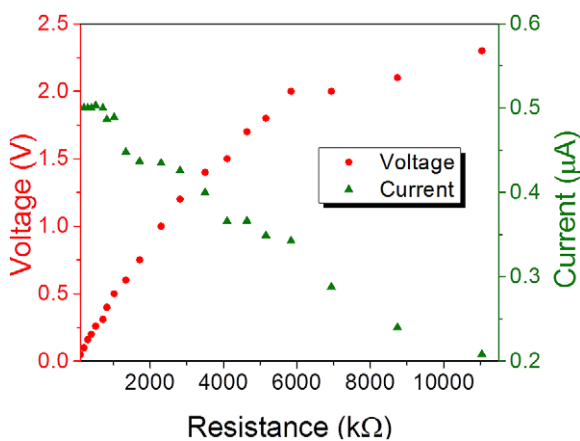


**Figure 9.** Output voltage and current characteristics of the TEH at different resistance values.

acceleration level of 1 g. As the load resistance is increased, the power output increases upto optimum value of load resistance and starts decreasing thereafter. The optimum value of

load resistance was observed to be 5.8 MΩ. Time domain signals of the TEH at the optimum value of resistance were also recorded, as shown in figure 10(b) and 10(c).

#### 4.5. Effect of PDMS micropad array configuration on device performance

Topography of the triboelectric layer can have a profound effect on the contact electrification effect. To study the effect of PDMS micropad array configuration, five sets of TEH devices were assembled on the shaker and tested. Time domain results for open circuit voltages for all five devices tested are shown in figure 11. It is interesting to notice that the overall primary contact area due to PDMS micropad cross section remains the same as discussed in section 4.2. Also, after the elastic deformation of PDMS micropads the overall contact area should theoretically remain the same for same value of applied mechanical stress. This has been discussed in the section 3.1. It was observed that although the overall contact area remains the same before and after the elastic deformation in PDMS micropads,

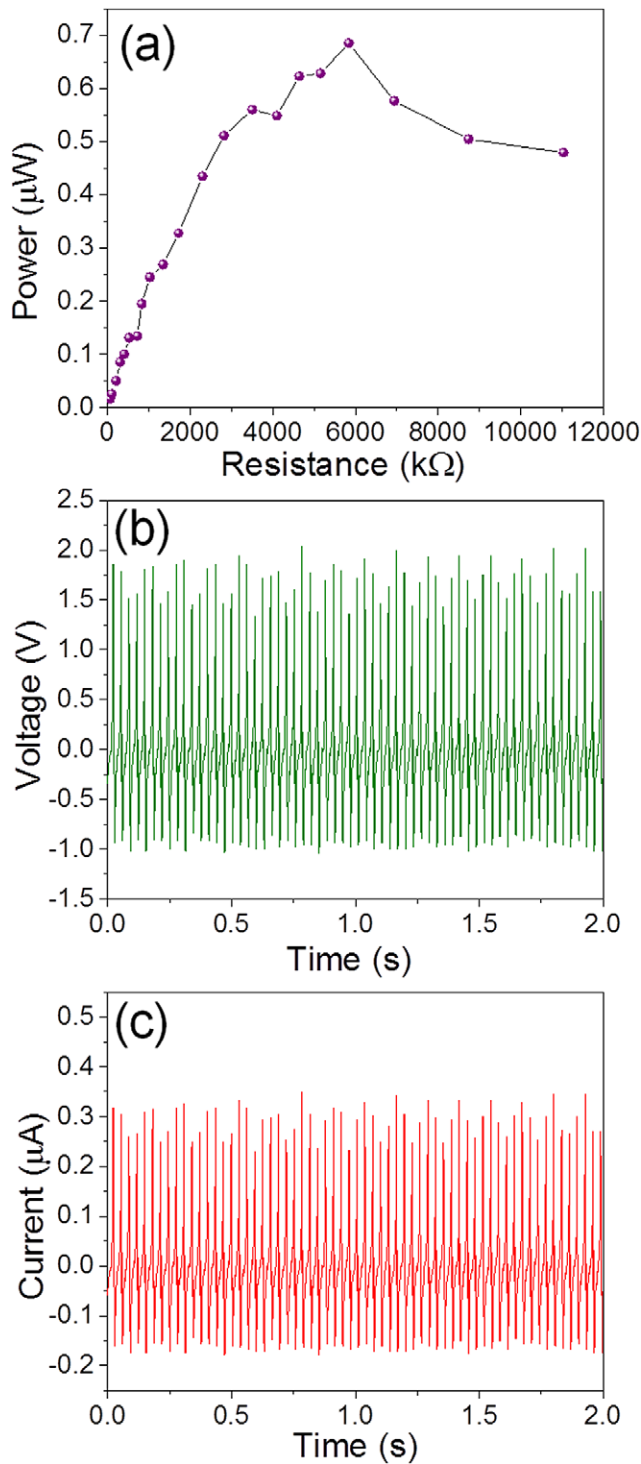


**Figure 10.** (a) Power characteristics of the TEH at different values of resistances. (b) Open circuit voltage at optimal load resistance of 5.84 MΩ. (c) Short circuit current at optimal load resistance of 5.84 MΩ.

the array configurations which used the micropad cross section area divided into smaller micropads had a relatively better performance compared to bigger micropads with same overall contact area. This device behavior can be explained by the easier separation of the triboelectric charge [20] when there are sharper or smaller asperities keeping the overall contact area between the two triboelectric layers the same. This result

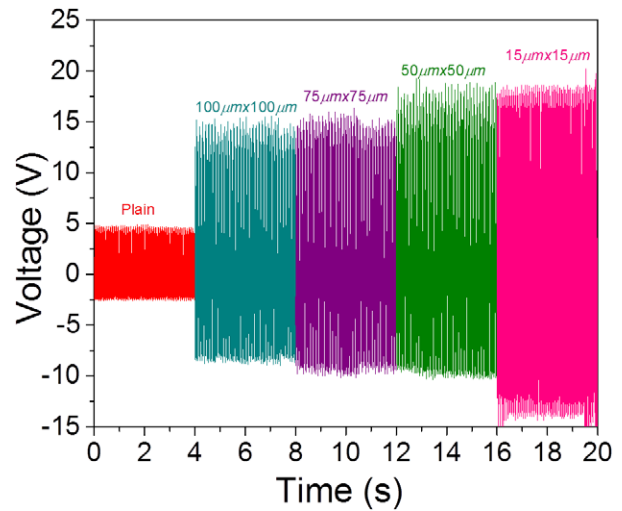


**Figure 11.** Comparison of time domain signals from different micropad cross-section samples.

is important and can possibly be extended to further topographies. This means if it is possible to pattern the triboelectric layer with similar materials with smaller dimension structures keeping the overall contact area same, the device performance of triboelectric mechanism based energy harvesters can be greatly improved.

*4.6. Testing of the TEH using a piezoelectric bimorph demonstrating hybrid energy harvesting mechanism*

Experiments were conducted to study the performance of piezoelectric and triboelectric energy harvesting mechanism operating simultaneously under similar acceleration and force levels. To setup the experiment, the aluminum cantilever used in experiments to test TEH, as discussed in previous sections, was replaced by a commercially available piezoelectric bimorph (from Steiner & Martins Inc.). The resonant frequency of the bimorph assembled with the first triboelectric layer and additional proof mass of 2.36 gram was found to be about 25 Hz. The hybrid energy harvester was then tested at a constant acceleration of 1 g. The time domain signals observed are shown in figure 12(a). The peak voltage generated by the piezoelectric energy harvester (PEH) was ~9V and the peak voltage generated by the TEH was observed to be ~4V. The PEH peaks in time domain as shown in figure 12(a) are broader unlike that of TEH which has characteristically very sharp peaks. The broader peaks of PEH would result in higher overall power as compared to TEH’s sharp peaks even if the peak voltage generated by both mechanisms are same. It is also worth noticing that PEH time domain output signals are not symmetric with respect to the time-axis. The reason for the non-symmetrical signal is the incomplete vibration cycle of the piezoelectric bimorph when it moves towards the second triboelectric layer after crossing the zero-stress position. The first triboelectric layer then comes in contact with the second triboelectric layer and limits the piezoelectric bimorph’s motion, which results in higher peaks of PEH output on the positive side of the time axis, as

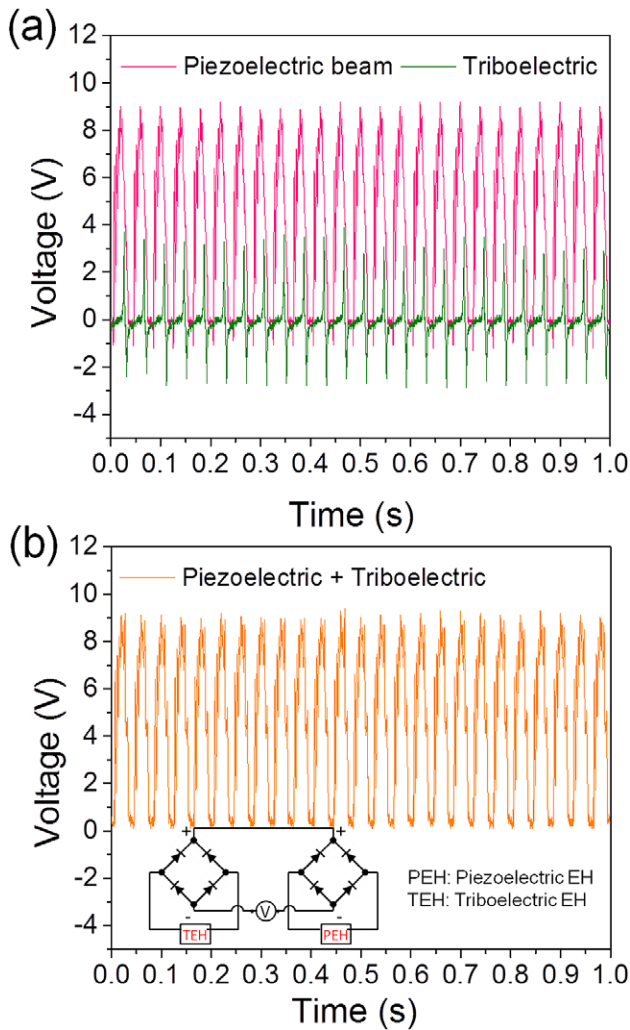


**Figure 12.** (a) Time domain signal of the voltage output from TEH and piezoelectric bimorph (PEH) (b) Time domain signal for rectified signal from TEH and PEH connected in series with same polarity.

shown in figure 12(a). Both signals are then added in same polarity after rectifying the signal using a rectifying circuit, as shown in figure 12(b). Adding the signals from TEH and PEH resulted in broader and taller peaks in time domain and hence increased overall power output from the hybrid mechanism.

The proposed hybrid mechanism using a triboelectric and piezoelectric mechanism can be a possible solution for improved power output with broadband characteristics at low frequencies. In the current hybrid mechanism, the piezoelectric mechanism has a better output than the triboelectric mechanism. Further optimization of the triboelectric mechanism using better material combination and topography would result in significant improvement of TEH performance leading to better output from hybrid energy harvesting devices.

## 5. Conclusion

A study has been conducted using elastic PDMS micropad structures on the performance of triboelectric energy harvesting mechanism. The performance of smaller structures

keeping the overall contact area constant between two triboelectric layers is found to be better as compared to relatively bigger structures. The mechanism used has also been shown to demonstrate broadband behavior for resonant mechanism based energy harvesting devices. A theoretical model has been developed for working out the triboelectric mechanism and the broadband behavior of the device.

The optimum peak power output of the TEH was obtained to be  $0.69 \mu\text{W}$  at an acceleration level of 1 g with an additional proof mass of 2.36 gram at the cantilever tip. The improvement in operating bandwidth of the TEH is demonstrated to be 63% at an acceleration of 1 g. A hybrid energy harvesting mechanism has also been proposed which uses triboelectric and piezoelectric mechanisms concurrently to improve the overall performance of the device.

## Acknowledgements

This work is partially supported by the Faculty Research Committee (FRC) Grant (No. R-263-000-692-112) at the National University of Singapore, and the NRF2011 NRF-CRP001-057 Program 'Self-powered body sensor for disease management and prevention-orientated healthcare' (R-263-000-A27-281) from the National Research Foundation (NRF), Singapore.

## References

- [1] Paradiso J A and Starner T 2005 Energy scavenging for mobile and wireless electronics *Pervasive Comput. IEEE* **4** 18–27
- [2] Mitcheson P D, Yeatman E M, Rao G K, Holmes A S and Green T C 2008 Energy harvesting from human and machine motion for wireless electronic devices *Proc IEEE* **96** 1457–86
- [3] Ottman G K, Hofmann H F, Bhatt A C and Lesieutre G A 2002 Adaptive piezoelectric energy harvesting circuit for wireless remote power supply *Power Electron. IEEE Trans.* **17** 669–76
- [4] Torah R, Glynne-Jones P, Tudor M, O'Donnell T, Roy S and Beeby S 2008 Self-powered autonomous wireless sensor node using vibration energy harvesting *Meas. Sci. Technol.* **19** 125202
- [5] Howells C A 2009 Piezoelectric energy harvesting *Energy Conversion Manag.* **50** 1847–50
- [6] Elfrink R et al 2009 Vibration energy harvesting with aluminum nitride-based piezoelectric devices *J. Micromech. Microeng.* **19** 094005
- [7] Goldschmidtboeing F and Woias P 2008 Characterization of different beam shapes for piezoelectric energy harvesting *J. Micromech. Microeng.* **18** 104013
- [8] Lee B, Lin S, Wu W, Wang X, Chang P and Lee C 2009 Piezoelectric MEMS generators fabricated with an aerosol deposition PZT thin film *J. Micromech. Microeng.* **19** 065014
- [9] Erturk A and Inman D J 2009 An experimentally validated bimorph cantilever model for piezoelectric energy harvesting from base excitations *Smart Mater. Struct.* **18** 025009
- [10] Shu Y and Lien I 2006 Analysis of power output for piezoelectric energy harvesting systems *Smart Mater. Struct.* **15** 1499

- [11] Beeby S P *et al* 2007 A micro electromagnetic generator for vibration energy harvesting *J. Micromech. Microeng.* **17** 1257
- [12] Wang P, Tanaka K, Sugiyama S, Dai X, Zhao X and Liu J 2009 A micro electromagnetic low level vibration energy harvester based on MEMS technology *Microsystem Technol.* **15** 941–51
- [13] Saha C, O'donnell T, Wang N and McCloskey P 2008 Electromagnetic generator for harvesting energy from human motion *Sensors Actuators A* **147** 248–53
- [14] Khan F, Sassani F and Stoerber B 2010 Copper foil-type vibration-based electromagnetic energy harvester *J. Micromech. Microeng.* **20** 125006
- [15] Glynn-Jones P, Tudor M, Beeby S and White N 2004 An electromagnetic, vibration-powered generator for intelligent sensor systems *Sensors Actuators A* **110** 344–9
- [16] Tvedt L G W, Nguyen D S and Halvorsen E 2010 Nonlinear behavior of an electrostatic energy harvester under wide- and narrowband excitation *J. Microelectromech. Sys.* **19** 305–16
- [17] Basset P, Galayko D, Paracha A M, Marty F, Dudka A and Bourouina T 2009 A batch-fabricated and electrode-free silicon electrostatic vibration energy harvester *J. Micromech. Microeng.* **19** 115025
- [18] Zhu G *et al* 2012 Triboelectric-generator-driven pulse electrodeposition for micropatterning *Nano Lett.* **12** 4960–5
- [19] Fan F-R, Tian Z-Q and Lin Wang Z 2012 Flexible triboelectric generator *Nano Energy* **1** 328–4
- [20] Fan F-R, Lin L, Zhu G, Wu W, Zhang R and Wang Z L 2012 Transparent triboelectric nanogenerators and self-powered pressure sensors based on micropatterned plastic films *Nano Lett.* **12** 3109–14
- [21] Zhang X-S *et al* 2013 Frequency-multiplication high-output triboelectric nanogenerator for sustainably powering biomedical microsystems *Nano Lett.* **13** 1168–72
- [22] Meng B *et al* 2013 A transparent single-friction-surface triboelectric generator and self-powered touch sensor *Energy Environ. Sci.* **6** 3235–40
- [23] Meng B, Cheng X, Zhang X, Han M, Liu W and Zhang H 2014 Single-friction-surface triboelectric generator with human body conduit *Appl. Phys. Lett.* **104** 103904
- [24] Dhakar L, Tay F E H and Lee C 2014 Development of a broadband triboelectric energy harvester with SU-8 micropillars *J. Microelectromech. Sys.* **PP** 1
- [25] Lu Y, Wang X, Wu X, Qin J and Lu R 2014 A non-resonant, gravity-induced micro triboelectric harvester to collect kinetic energy from low-frequency jiggling movements of human limbs *J. Micromech. Microeng.* **24** 065010
- [26] Zhu G *et al* 2013 Toward large-scale energy harvesting by a nanoparticle-enhanced triboelectric nanogenerator *Nano Lett.* **13** 847–53
- [27] Henniker J 1962 Triboelectricity in polymers *Nature* **196** 474
- [28] Park C H, Park J K, Jeon H S and Chun B C 2008 Triboelectric series and charging properties of plastics using the designed vertical-reciprocation charger *J. Electrostat.* **66** 578–83
- [29] Sebald G, Kuwano H, Guyomar D and Ducharme B 2011 Experimental duffing oscillator for broadband piezoelectric energy harvesting *Smart Mater. Struct.* **20** 102001
- [30] Stanton S C, McGehee C C and Mann B P 2010 Nonlinear dynamics for broadband energy harvesting: Investigation of a bistable piezoelectric inertial generator *Physica D: Nonlinear Phenom.* **239** 640–53
- [31] Xue H, Hu Y and Wang Q-M 2008 Broadband piezoelectric energy harvesting devices using multiple bimorphs with different operating frequencies *Ultrason. Ferroelectr. Freq. Control IEEE Trans.* **55** 2104–8
- [32] Nguyen S D and Halvorsen E 2011 Nonlinear springs for bandwidth-tolerant vibration energy harvesting *J. Microelectromech. Sys.* **20** 1225–7
- [33] Soliman M S M, Abdel-Rahman E M, El-Saadany E F and Mansour R R 2008 A wideband vibration-based energy harvester *J. Micromech. Microeng.* **18** 115021
- [34] Wang Z L and Wu W 2012 Nanotechnology-enabled energy harvesting for self-powered micro-/nanosystems *Angew. Chem. Int. Edn.* **51** 11700–21
- [35] Chandra D and Yang S 2010 Stability of high-aspect-ratio micropillar arrays against adhesive and capillary forces *Accounts of Chem. Res.* **43** 1080–91
- [36] Stronge W J 2004 *Impact Mechanics* (Cambridge: Cambridge University Press)
- [37] Matsusaka S, Ghadiri M and Masuda H 2000 Electrification of an elastic sphere by repeated impacts on a metal plate *J. Phys. D: Appl. Phys.* **33** 2311
- [38] Niu S *et al* 2013 Theoretical study of contact-mode triboelectric nanogenerators as an effective power source *Energy & Environ. Sci.* **6** 3576–83
- [39] Dhakar L, Liu H, Tay F and Lee C 2013 A new energy harvester design for high power output at low frequencies *Sensors Actuators A* **199** 344–52
- [40] Liu H, Lee C, Kobayashi T, Tay C J and Quan C 2012 Investigation of a MEMS piezoelectric energy harvester system with a frequency-widened-bandwidth mechanism introduced by mechanical stoppers *Smart Mater. Struct.* **21** 035005